PHOTONICS Research

Photonic smart bandage for wound healing assessment

Arnaldo Leal-Junior,[1,5] Jingjing Guo,[2,*] Rui Min,[3] António José Fernandes,[4] Anselmo Frizera,[1] and Carlos Marques[4]

[1]Telecommunications Laboratory (LABTEL), Graduate Program in Electrical Engineering, Federal University of Espírito Santo, Vitória-ES 29075-910, Brazil
[2]School of Instrumentation and Optoelectronic Engineering, Beihang University, Beijing 100191, China
[3]Center for Cognition and Neuroergonomics, State Key Laboratory of Cognitive Neuroscience and Learning, Beijing Normal University, Zhuhai 519087, China
[4]Physics Department & I3N, Universidade de Aveiro, Campus Universitário de Santiago, Aveiro 3810-193, Portugal
[5]e-mail: leal-junior.arnaldo@ieee.org
*Corresponding author: guojj13@126.com

Received 14 September 2020; revised 28 October 2020; accepted 3 November 2020; posted 3 November 2020 (Doc. ID 410168); published 5 February 2021

Chronic wounds affect around 2% of the world population with an annual multi-billion dollar cost to the healthcare system. This background pushes the development of new therapies and procedures for wound healing and its assessment. Among them, the potential of hydrogen (pH) assessment is an important indicator of the wound healing stage and condition. This paper presents the development of the first optical fiber-embedded smart wound dressing for pH assessment. An intrinsically pH-sensitive optical fiber is fabricated using a polydimethylsiloxane (PDMS) precursor doped with rhodamine B dye. Raman and Fourier transform infrared (FTIR) spectroscopies are performed in order to verify the presence of rhodamine B and PDMS in the fiber samples. Then, the fiber is embedded in gauze fabric and hydrocolloid wound dressing. In addition, such low Young's modulus of PDMS fiber enables its use as a highly sensitive pressure sensor, where the results show that the fiber-embedded bandage can measure pressures as low as 0.1 kPa with a high linearity in the range of 0 to 0.3 kPa. The smart bandage is subjected to different pH, which resulted in a wavelength shift of 0.67 nm/pH when the absorption peak at 515 nm was analyzed. Furthermore, pH increase leads to linear decrease of the transmitted optical power (R^2 of 0.998), with rise and fall times below 20 s and 30 s, respectively. Therefore, the proposed optical fiber-embedded smart bandage enables the simultaneous assessment of pressure and pH on the wound region. © 2021 Chinese Laser Press

https://doi.org/10.1364/PRJ.410168

1. INTRODUCTION

From the beginning to the end of a life cycle, physical injuries commonly occur with most of the population. Such injuries can result in skin damage and wounds. Despite a multitude of accidental injuries, wounds can also be related to pressure ulcers, diabetes foot ulcers, and other underlying diseases [1]. If the wound does not restore anatomic and functional integrity within three months, it becomes a chronic wound [2]. Recent studies indicate that around 2% of the world population suffers from chronic wounds [2]. Such widespread chronic wounds result in an economic burden to the healthcare system with an annual cost of multi-billions of dollars [1].

The mortality resulting from complications in chronic wounds (e.g., infections and septicaemia [1]) raises a big concern in the medical community, which also refers to chronic wounds as a "silent epidemic" with its main cause related to inadequate planning and implementation of prevention, treatment, and management [2]. To that extent, new treatments [3], protocols, and procedures [4] have been reported. Some of these new treatments mainly rely on the development of novel biomaterials with antibacterial and anti-oxidant properties for wound dressing, promoting an accelerated healing [5]. Among these new materials for wound healing, hydrogels are commonly explored with important advantages of self-healing, as well as extensibility due to their favorable mechanical properties [6].

To address the wound healing and the functionalities of new healing treatments, quantitative indicators for the assessment of wound healing are needed. In this case, the potential of hydrogen (pH) in the wound and its influence on the healing process have been investigated throughout the years [7]. The human skin has an acidic pH in the range of 4 to 5.5 with its exact

value depending on the person's age and the anatomic location [8]. Alkaline pH in wound beds contributes to the growth and spread of pathogenic bacteria, which leads to poor healing conditions [7]. The wound healing process comprises four phases, i.e., haemostasis, inflammation, proliferation, and remodeling [7]. An acidic milieu is beneficial for wound healing, since it provides an unsuitable environment for pathogenic bacteria proliferation and improves the tissue oxygenation, a key factor for successful wound healing [8]. Furthermore, the wound pH is an indicator of its healing process, since, in its early condition, the wounds have a slightly alkaline pH (circa 7.6), which become neutral and, then, acidic as the healing process evolves [7]. For these reasons, many wound care therapies such as wound dressing, including the ones based on hydrocolloids, focus on the pH modification on the wound region [9]. In addition, some new wound treatments indicate that the pressure applied on the wound can affect its healing [10]. Thus, the measurement of the pressure applied to the wound region can assess the wound condition in the treatments that involve mechanical forces on the wounded region. Moreover, pressure monitoring in the skin can also anticipate and/or monitor pressure ulcers [1].

As the pH in the wound region is an important indicator of the wound healing (and treatment effectiveness), different wearable techniques for measuring pH in wounds were recently proposed [11]. The reported techniques include colorimetric detection using pH-sensitive films [12]. In another approach, Du and Ciou [13] reported a wearable sensor for the assessment of moisture and pH in wounds, where a multi-channel system measures the moisture and pH through moisture and pH-sensitive films that create potential difference in the electric signals with pH and moisture variations with the inherently electromagnetic field dependency of such systems. In contrast, optical fiber sensors experience a widespread operation especially due to its possibility of embedment in different structures (from concrete to clothing/textiles) as well as intrinsic safe operation, where there are only optical signals in the sensing region [14], which make them suitable for biomedical and healthcare applications [15]. Additional advantages of optical fiber sensors include compactness, multiplexing capabilities, galvanic isolation, and electromagnetic field immunity, which motivate the development of a large range of sensors covering physical and chemical parameters, including pH sensors [16]. Optical fiber-based pH sensors have been proposed using conventional silica optical fibers [17] and polymer optical fibers (POFs) [18] with sensor approaches such as gratings (uniform [16] and tilted [19]), surface plasmon resonance [20], interferometers [17], and fluorescence [21]. As commercially available optical fibers are not intrinsically sensitive to pH, the fabrication of these sensors includes the use of sensitive films [19], hydrogel coatings [18], or pH-sensitive dyes [21].

The advances in polymer processing technology enable the development of new POFs made of different materials with important features such as high flexibility [22,23], biocompatibility [23], and biodegradability [24]. Among these new fibers, Guo *et al.* [25] proposed a highly flexible optical fiber for wearable applications. Such fiber was also used as wearable strain sensor [26]. This fiber comprises a polydimethylsiloxane (PDMS) matrix doped with rhodamine B, where the latter can be used as a pH fluorescent indicator [27], which results in the first pH-sensitive optical fiber. In addition, the high flexibility of the PDMS fiber enables its embedment in textiles and wound dressing without influencing their stiffness. Considering these functionalities, this paper presents the development of the first optical fiber-embedded smart wound dressing for pH assessment in wounds. The dye-doped PDMS fiber is embedded in the gauze's fabric and in a hydrocolloid wound dressing, each one with its own benefits for wound treatment. Raman and infrared spectroscopies are applied in the fiber to verify its composition, and the mechanical characterization is performed in the fiber and wound dressing materials in order to verify the influence of the PDMS fiber in the smart wound dressing stiffness. In addition, the pressure sensitivity of the proposed system is characterized. Then, the pH assessment of the proposed smart bandage is performed, and the sensing possibilities (including the simultaneous assessment of pressure and pH) using the proposed smart system are discussed. The contributions of this work are not only the development of the first photonic smart bandage that provides the possibility of important advances in wound healing assessment, but also the new possibilities of simultaneous physical and chemical sensing using a dye-doped PDMS fiber with remarkable flexibility suitable for highly sensitive physical sensing and the intrinsic pH sensitivity that results in many possibility of chemical sensing approaches. Thus, with the design and results of the proposed optical fiber-embedded smart bandage, it is possible to envisage a next generation of smart wound dressings in which a real-time assessment of the wound healing brings novel paradigms for wound treatments and can dramatically enhance the treatment efficiency.

2. EXPERIMENTAL SECTION

A. Fiber Fabrication and Wound Dressing Integration

The fiber is fabricated using PDMS precursors comprised of the monomer and curing agent (Dow Corning, Slygard 184) in the proportion of 10:1. Furthermore, the rhodamine B dye molecules are added in the mixture, which is injected into a silicone tube with 0.5 mm diameter. The curing occurs at 80°C for 40 min, and additional details for the fiber fabrication are presented by Guo *et al.* [25]. The demolding process is performed by injecting water in the silicone tube using a syringe connected to the silicone tube, where the PDMS fiber demolding is achieved through the water pressure in the fiber end facet. The PDMS fiber has 0.5 mm diameter, and 30 mm long fibers were used in the bandage embedment. A rhodamine B doping concentration of $2.5 \times 10^{-4}\%$ (w/v) was used, which increases the optical losses in the fiber, resulting in an optical loss of around 3 dB/cm for this fiber. For this reason, the sensor is limited to short lengths of fiber in order to use low-power optical sources. Thereafter, the optical fiber was embedded in the bandages. For the gauze fabric embedment, the fiber is sewed between two layers of the gauze fabric, where the stiches are placed in the inner layers of the fabric in a manner that they are neither visible nor in contact with the wound region. For the embedment in the hydrocolloid dressing, two 0.5 mm diameter holes with 10 mm separation between them were

made on the dressing for the PDMS fiber embedment and positioning.

B. Raman Spectroscopy and FTIR

The Raman spectroscopy is performed on the fiber end facet, which was cleaved at 90° using a sharp blade and, then, positioned on the Raman confocal microscope. The micro-Raman spectrum is obtained in the backscattering configuration using a monochromatic light source (LS, 442 nm) from a He:Cd laser with a 50× objective lens (NA 0.7) resulting in a spot diameter of ∼2 μm focused on the fiber center. In contrast, the Fourier transform infrared (FTIR) measurements were performed in the fiber samples to verify the presence of PDMS and rhodamine B in the molecular structure. In this case, the samples are cut into micrometer-scale pieces, which are positioned on a crystal plate of 1 mm^2, and the transmittance spectrum is obtained as a function of the wavenumber for the attenuated total reflection probe, where the evanescent wave resulting from the total internal reflection on the sample is analyzed.

C. Tensile Tests

The tensile tests are performed using a universal testing machine equipped with a linear variable differential transformer (LVDT) sensor for displacement assessment and a load cell for the force measurement. The samples (dye-doped PDMS fiber, gauze fabric, and hydrocolloid dressing) are positioned on the tensile machine's clamps. Then, a constant strain rate of 10 mm/min is applied with the strain (related with the displacement) and the stress (force) continuously monitored. The Young's modulus of each material is estimated through the slope of the stress-strain curve in the elastic region according to the ISO 527-1:2019 for tensile properties evaluation in plastics.

D. Experimental Setup for Pressure and pH Monitoring

For pressure and pH monitoring, two experimental setups are used, one for the continuous assessment of optical power variations and the other for the transmitted optical spectrum acquisition. In both approaches, a white LS with 3 mW optical power is employed. In addition, the PDMS fiber is connected to multimode POF on both ends (one to the LS and the other to the detector). The connection is made by aligning both fibers, after which a UV-curable resin is applied on the interface between fibers and cured using a UV lamp. The continuous monitoring of the transmitted optical power is achieved by connecting the fiber to a photodetector (PD) IF-D92 (Industrial Fiber Optics, USA) whose signal is acquired by a microcontroller FRDM-KL2Z (NXP, The Netherlands) with a 16-bit analog-to-digital converter. The spectrometer USB2000+ (Ocean Optics, USA) with 400 nm to 700 nm range and 0.1 nm accuracy is employed for the transmitted optical spectrum acquisition.

The pressure characterization is performed by positioning the smart bandage (with the experimental setup described above) on a fixed platform in which blocks with calibrated mass and known area are positioned above the bandage. Considering the blocks mass and area, the pressures applied on the sensor are about 0.1 kPa, 0.15 kPa, 0.2 kPa, 0.25 kPa, and 0.3 kPa, where each pressure is applied for 15 s in three consecutive cycles. The mean and standard deviation of the sensor responses on each test are analyzed and compared with the applied pressure.

The pH responses of the proposed sensor system are characterized by placing the smart bandage inside a container filled with buffer solutions of different pH (ranging from pH 4 to 7), where the pH of each solution is measured using a portable pH meter with dynamic ranges that cover the pH range (0–14) and a measurement precision of ±0.02 pH for comparison purposes. The optical fiber-embedded wound dressing is submerged into each solution for about 120 s, where the mean and standard deviation of each test are analyzed as a function of the solution pH. For the dynamic pH variations, the smart bandage is placed inside the container filled with acidic buffer solution (pH 4), and neutral buffer solution is added while the pH is monitored using the pH meter. In this case, the pH value is increased and, then, decreased, whereas the rise and fall times as well as pH stabilization are analyzed using the proposed sensor system.

3. RESULTS AND DISCUSSION

The optical fiber has a dye-doped PDMS core/cladding in which a rhodamine B dye is added in the PDMS precursor before its thermal curing. The rhodamine B dye has wavelength-dependent absorption/fluorescence and is pH sensitive due to its structural changes when subjected to different pH values. In fact, acidic pH results in spirolactam ring opening of the rhodamine B structure, whereas such a ring remains closed under neutral or alkaline conditions. The spirolactam ring opening leads to a fluorescence increase [28], which can be used as a pH indicator in neutral and acidic environments such as the one in the wounds [12]. Thus, the pH sensing with the proposed optical fiber-embedded smart bandage is based on the interaction between the rhodamine B dye and the environmental pH, i.e., that in the wound region where the smart bandage is positioned, as depicted in Fig. 1(a). In addition, the PDMS fiber has a low Young's modulus, which, in conjunction with its small dimensions (0.5 mm diameter), results in an optical fiber with low stiffness. Such stiffness is comparable with the ones of the bandage materials, even when highly flexible bandages are used, such as the hydrocolloid one, where this feature is demonstrated through the tensile tests presented later in this section. It is also worth noting that the PDMS fiber is sensitive to pressure (or strain) applied on the bandage. Pressure or transverse strain applied on the optical fiber can lead to macrobending and the stress-optic effect (refractive index variation proportional to the applied stress), which result in variations in the transmitted optical power [29]. Furthermore, the variation in the transmitted optical power is also related to absorption changes in the dye due to the strain. For this reason, it is possible to estimate the pressures applied on the wound region, which can affect its healing [10]. In addition, as shown in Fig. 1(b), a system with multiple fibers can simultaneously measure pressure and pH [represented in Fig. 1(b) as P and pH, respectively], where the dye-doped PDMS fiber is connected to two multimode fibers (MMFs): one connected to the PD and the other to the LS. Another possibility for simultaneous assessment of pressure and pH is through the analysis of the wavelength shift and optical power variation in the

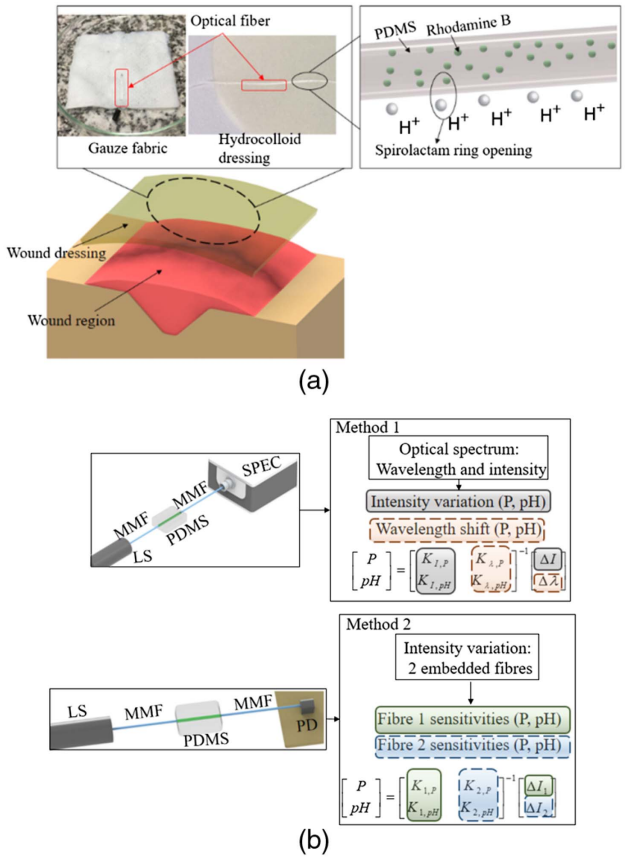

Fig. 1. (a) Schematic representation of the proposed optical fiber-embedded smart bandage. (b) The fiber embedded in gauze fabric and hydrocolloid dressing is shown, and two techniques for simultaneous assessment of pressure and pH are shown (using two embedded fibers and the transmitted spectrum analysis). LS, light source; MMF, multimode fiber; PDMS, dye-doped PDMS fiber; PD, photodetector; SPEC, spectrometer.

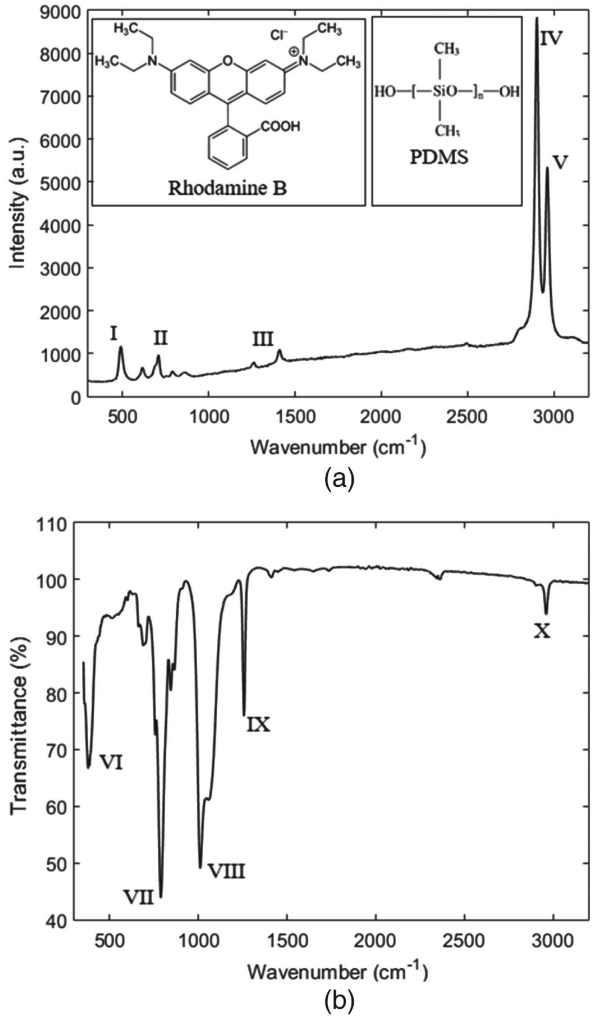

Fig. 2. (a) Raman and (b) infrared spectra of the dye-doped PDMS optical fiber. Figure inset shows the molecular structures of PDMS and rhodamine B.

transmitted optical spectrum acquired by a spectrometer [represented as SPEC in Fig. 1(b)].

The molecular structure of the dye-doped PDMS optical fiber is assessed through Raman spectroscopy and FTIR spectroscopy. In micro-Raman spectroscopy, the spectra are obtained from the inelastic scattering of light due to its interaction with the material's vibrational dynamics, enabling the identification of the molecular structures locally by focusing the laser beam (~2 μm spot size). In this case, the confocal Raman microscope is focused in a micrometer-scale region at the center of a PDMS fiber end facet. Figure 2(a) shows the Raman spectrum of the sample. Considering the chemical structure of PDMS and rhodamine B (shown in Fig. 2), the Raman spectrum shows features of both structures, where the peak around 500 cm^{-1} (peak I) is related to Si–O–Si bond, whereas the one at 800 cm^{-1} (peak II) is related and Si–CH_3 bond, both assigned to the PDMS structure. In addition, there are peaks at 1350 cm^{-1} and 2800 cm^{-1} (peaks III and IV, respectively) due to C–N and N–CH_3 bonds, respectively [30], corresponding to vibrational modes of rhodamine B. It is also worth to mention that bands related to stretching and bending modes common to both structures (PDMS and rhodamine B), such as the C–H stretching in CH_3 at 3000 cm^{-1} (peak V), are also present. As a complementary approach for the Raman spectrum shown in Fig. 2(a), FTIR spectroscopy analysis was also undertaken in the optical fiber, where the vibration modes that change the dipole moment of a structure are visible in the infrared spectrum shown in Fig. 2(b). In FTIR spectroscopy, the fiber was cut into sub-micrometer-scale pieces and positioned on a crystal plate, where the transmittance spectrum was obtained using an attenuated total reflection probe. The results show peaks related to the rhodamine B structure, which include the C–N, N–CH_3, and aromatic rings, at 1300 cm^{-1} (peak IX), 2800 cm^{-1} (peak X), and 1060 cm^{-1} (peak VIII), respectively, whereas peaks related to the PDMS bonds such as Si–O–Si and Si–CH_3 are observable at 500 cm^{-1} (peak VI) and 800 cm^{-1} (peak VII), respectively. Thus, both spectroscopic techniques unequivocally confirm the presence of both PDMS and rhodamine B dye in the optical fiber used on the bandage embedment.

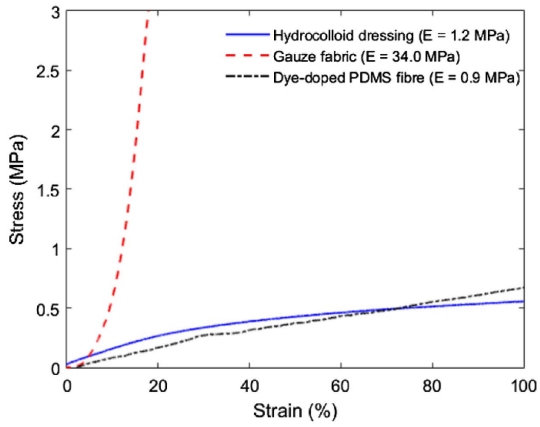

Fig. 3. Experimental stress-strain curves of the hydrocolloid dressing, gauze fabric, and dye-doped PDMS fiber.

Then, the mechanical properties of the materials (dye-doped PDMS fiber, gauze fabric, and hydrocolloid dressing) are characterized in the tensile tests in which the same strain rate (10 mm/min) is applied for all samples. Figure 3 shows the stress-strain and force-displacement curves for all analyzed materials obtained in experimental results using the methods described in Section 2.C. Comparing the results, the gauze fabric showed the highest slope on the stress-strain curve, indicating a higher Young's modulus (and stiffness) than the hydrocolloid dressing and PDMS fiber. The hydrocolloid dressing and PDMS fiber presented similar slopes on their stress-strain curves, and both materials were capable of withstanding strains as high as 100%. Such low stiffness of the PDMS fiber indicates its suitability for the embedment in gauze fabric and even for the hydrocolloid dressing, since the proposed fiber does not change the stiffness of the wound dressing in both analyzed cases, i.e., gauze fabric and hydrocolloid dressing.

The small Young's modulus and stiffness of the optical fiber (see Fig. 3) are good indications for the proposed optical fiber-embedded smart bandage, since lower Young's modulus generally results in high pressure sensitivity [22]. In order to verify the pressure sensitivity of the proposed sensor, the smart bandage (with an embedded PDMS fiber) is positioned on a platform at which constant pressures are applied, whereas the fiber is illuminated with an LS and a PD acquires the optical power variation as a function of the pressure. Figure 4 shows the pressure response of the dye-doped PDMS fiber, where the time-domain sensor response under a constant pressure of 0.32 kPa (commonly applied in the interaction with human skin and in pressure treatments [31]) and the optical losses for different applied pressures are analyzed in Figs. 4(a) and 4(b), respectively. Such low-pressure detection is one important feature of this highly flexible fiber that is capable of detecting pressures with a resolution higher than most of the other optical fibers. The time-domain response indicates the reversibility of the fiber under pressure, where the solid and shaded lines represent the mean and standard deviation, respectively. The difference between the pressure loading and unloading is lower than 1%, which is below the standard deviation of the three performed tests [as shown in the shaded lines of Fig. 4(a)]. In addition, the

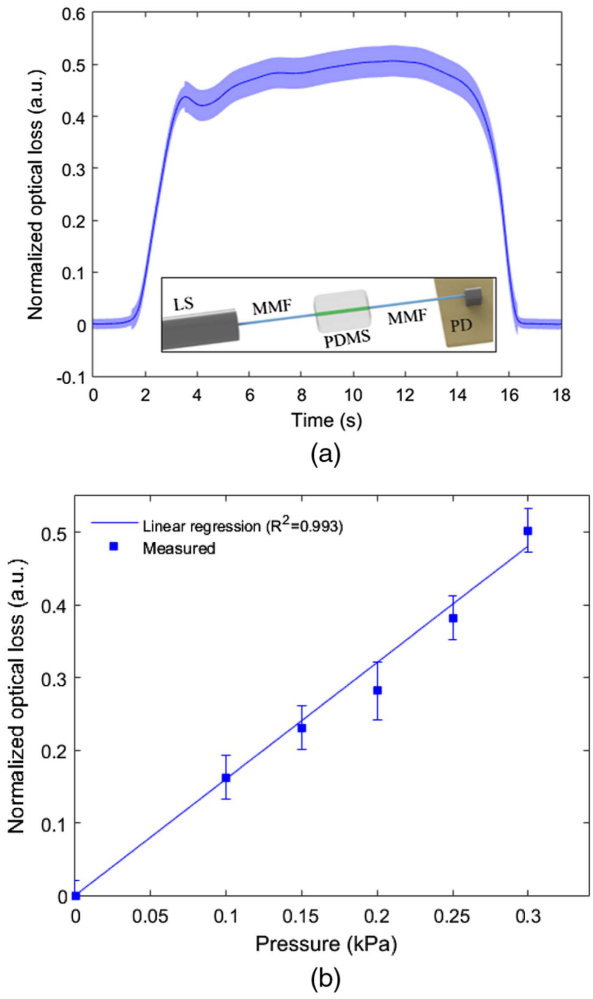

Fig. 4. (a) Transmitted optical power loss as a function of time for a constant pressure of 0.32 kPa. Shaded region represents the standard deviation in the pressure assessment. (b) Linear regression of the normalized optical loss as a function of the applied pressure.

PDMS fiber response under different pressure conditions shows high linearity as shown in Fig. 4(b), where a determination coefficient (R^2) of 0.993 is obtained with the possibility of measuring pressures as low as 0.1 kPa. Thus, the high flexibility of the fiber enables the assessment of pressures applied on the wound region (at which the smart bandage is positioned). Such pressure assessment is especially important in pressure ulcer monitoring [1] and for alternative treatments in chronic wounds that involve applying controlled pressure in the wound region [10].

In order to verify the spectral changes in the transmitted optical signal when the dye-doped PDMS fiber embedded in the hydrocolloid dressing is subjected to pH variations, the fiber (illuminated with a white LS) is connected to a spectrometer. Figure 5 shows the transmitted optical spectra under neutral, alkaline, and acidic pH conditions (8, 7, 6, 5, and 4). The results show a slight redshift in the peak wavelength as the pH increases, i.e., as the solution pH becomes neutral, with a wavelength shift of about 2.0 nm when comparing the pH 4 and pH 7 solutions. However, the transmitted optical power

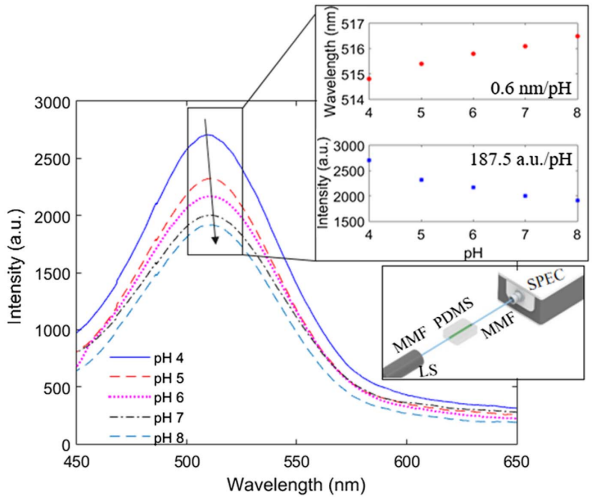

Fig. 5. Transmitted optical spectrum of the proposed smart bandage under three pH conditions. Figure insets show the intensity and peak wavelength as a function of the pH.

has high variation as a function of the pH, as can be observed by the vertical shift of the curves, where the transmitted optical power decreases monotonically with the pH increase. There is a smaller variation in alkaline pH, since the rhodamine B dye has a higher fluorescence in acidic environments.

The transmitted optical power variation as a function of the pH, as indicated in Fig. 5, motivates the pH assessment in the smart bandage using low-cost techniques for optical sensor signal demodulation. Thus, the optical losses as a function of the pH are analyzed with the dye-doped PDMS fiber connected to a PD. In this case, both smart bandages (fiber embedded in gauze fabric and hydrocolloid dressing) are tested under different pH conditions ranging from 4 to 7, as shown in Fig. 6(a). The sensors presented repeatability in all performed tests, where the results for three tests for each smart bandage presented a standard deviation below 5%. In addition, the high linearity of the proposed smart dressings is demonstrated, since the linear regression shows an R^2 of 0.998.

The gauze-embedded dye-doped PDMS fiber is also subjected to dynamic variations of the pH, where the results are shown in Fig. 6(b). In this case, the initial acidic pH of 4 was increased after 10 s to about 5.1 by the addition of a neutral solution and remained in such pH condition for about 30 s. Then, the pH decreased to 4.5 (by adding an acidic solution) with the sensor's stability evaluated for 120 s. The proposed sensor tracks all pH variations with high stability and reversibility. Furthermore, the optical fiber-embedded smart bandage is suitable for dynamic monitoring of pH, where a rise time of 19.0 s and a fall time of 18.9 s were obtained. It is worth noting that the pH increase and decrease were analyzed for different ranges (1.1 for the increase and 0.6 for decrease); normalizing the rise and fall times with respect to the pH variation, we obtain 17.2 s/pH and 31.5 s/pH for rise and fall, respectively. Moreover, the sensor shows a transmitted optical power variation of 2.4% at pH 5.1 (maintained for 30 s) and 4.0% at pH 4.5 for 120 s, where such variations result in a deviation of 0.05 on the pH assessment. This relatively short response time was

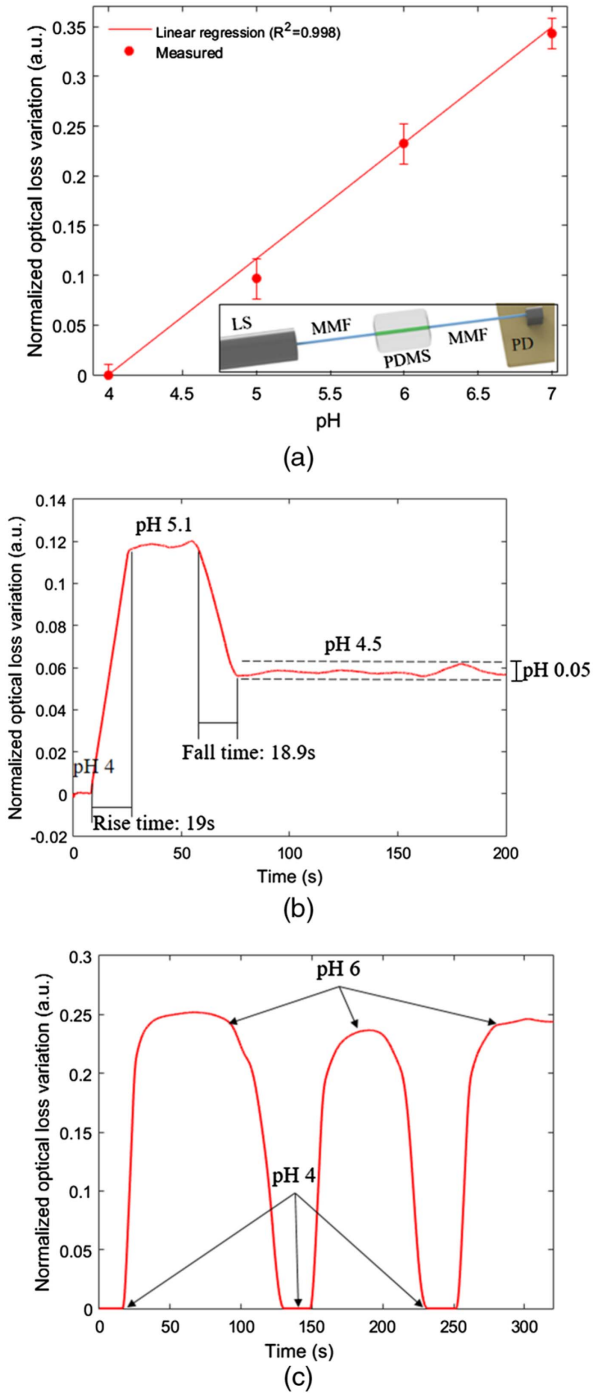

Fig. 6. (a) Linear regression of normalized optical loss variation as a function of the pH. (b) Sensor response under dynamic variations of pH, where the sensor stability and rise and fall times are presented. (c) Normalized optical loss variation as a function of time for cyclic pH variations from pH 4 to pH 6.

achieved due to the contact between the solution and the rhodamine B in the PDMS fiber. As shown in the Raman spectroscopy, where the laser was focused on the fiber surface, the presence of the rhodamine B was verified, indicating that the proposed optical fiber-embedded smart bandage is capable of detecting dynamic variations of the pH, especially for the

gauze-embedded sensor. Considering the hydrocolloid dressing and its swelling characteristic when subjected to the pH solutions, there is an increase in the response time of the proposed sensor when embedded in the hydrocolloid dressing. Thus, it is possible to consider that the response time for the hydrocolloid dressing is dependent not only on the dye-doped PDMS fiber response, indicated in Fig. 6(b), but also on the hydrocolloid dressing response time for moisture absorption and desorption. Moreover, the sensor stability is further verified in cyclic tests for pH variations from 4 to 6, as shown in Fig. 6(c). In this case, the sample was subjected to an acidic pH, which was increased using a buffer solution. Then, the sample was, once again, subjected to pH 4. This process was repeated three times, and the sensor response in Fig. 6(c) indicated that the sensor was capable of tracking the pH variations with short response time, similar to the one depicted in Fig. 6(b) and high stability, with only minor deviations in the transmitted optical power (below 5%) when each pH condition is reached.

The presented results indicate the feasibility of the proposed sensor for the assessment of pH and pressure. Although the sensor is sensitive to both parameters, different approaches can be adopted for the cross-sensitivity mitigation. Such techniques are also related to the interrogation principle used on the sensor analysis, since the proposed smart bandage can be interrogated using only the transmitted optical power variation (acquired by a PD) or by analyzing the transmitted optical spectrum (using a spectrometer). If only the transmitted optical power is analyzed, the pressure and pH response decoupling is obtained by embedding an additional fiber in the smart bandage. The pH and pressure sensitivities of this additional fiber can be characterized, and, since the sensor system shows a high linearity with respect to pressure and pH, both parameters can be simultaneously estimated by solving the linear system shown in Fig. 1(b), as also reported in the literature for simultaneous assessment of different parameters [32]. As another option for cross-sensitivity mitigation, the transmitted optical spectrum can be analyzed, instead of only the transmitted optical power. In this case, the peak wavelength is also analyzed, and this additional spectral feature enables the simultaneous assessment of pressure and pH, since they lead to different variations of transmitted optical power and peak wavelength. As shown in Fig. 5, the pH variation leads to wavelength shift in the transmitted spectrum, whereas the pressure does not lead to significant wavelength variations. It is also worth noting, by comparing the transmitted optical power as a function of pressure and pH, that they show different sensitivities. Thus, it is possible to estimate both parameters using one dye-doped PDMS fiber by analyzing additional spectral features, as shown in previous works [33] for simultaneous assessment of different parameters using only one sensor.

To verify the feasibility of the proposed techniques for simultaneous assessment of pressure and pH, additional tests are presented in Figs. 7(a) and 7(b). In this case, two samples are subjected to predefined pressure and pH using the methods described in Section 2.D. To decouple pressure and pH, both methods presented in Fig. 1(b) are used, where two sensors are employed. In Sensor 1, the wavelength shift and intensity are analyzed, whereas only the intensity is analyzed in Sensor 2. As

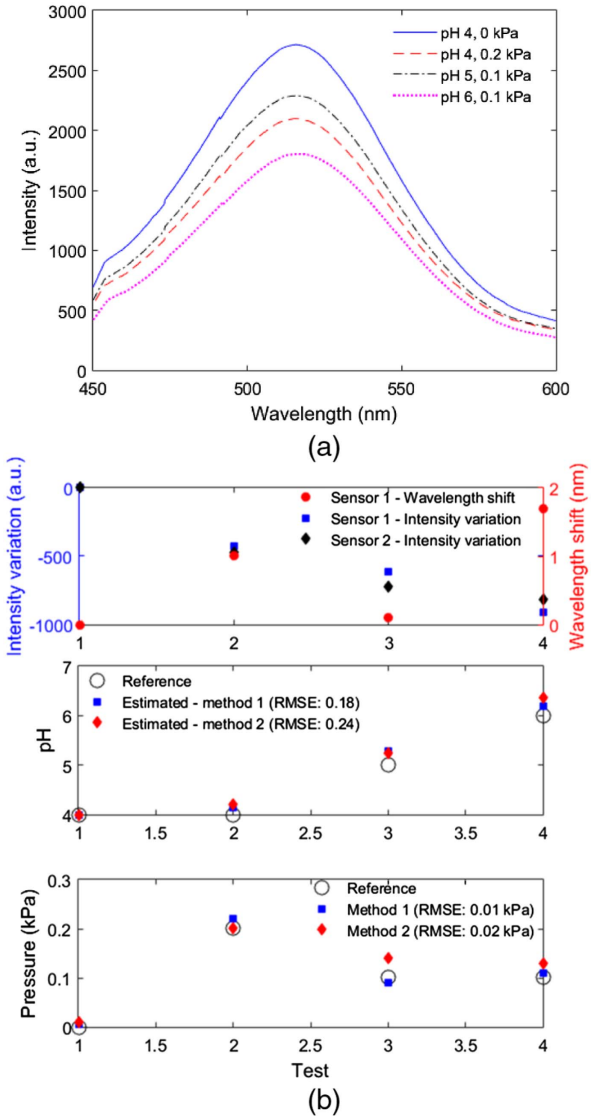

Fig. 7. (a) Transmitted spectra of Sensor 1 under different pressure and pH conditions. (b) Wavelength shift for Sensor 1 and intensity variation for Sensors 1 and 2. The pressure and pH estimation for each method is also presented and compared with the reference value of each parameter.

shown in Fig. 1(b), method 1 considers the wavelength shift and the intensity variation of Sensor 1 as a function of the pH and pressure, where each parameter is estimated from the linear regressions of both spectral features (wavelength shift and intensity) as a function of the desired parameters (pressure and pH, in this case) using the matrix shown in Fig. 1(b). In method 2, the intensity variations of Sensors 1 and 2 as a function of the simultaneous variations of pressure and pH are analyzed through the matrix presented in Fig. 1(b), resulting in pressure and pH estimations. Thus, as aforementioned, method 1 requires only one sensor, but also needs the analysis of the transmitted spectrum (wavelength and intensity), whereas method 2 needs two sensors, but only employs their intensity variations, which leads to the possibility of using low-cost PDs. For this reason, the wavelength shift of Sensor 2 was

not acquired. Figure 7(a) shows the transmitted spectra for various pressure and pH conditions, where pH variations from 4 to 6 and pressure variations from 0 to 0.2 kPa were applied. Figure 7(b) shows the intensity variations and wavelength shift of Sensor 1 and the intensity variation of Sensor 2. The root mean squared error (RMSE) of the pressure and pH estimations with each method is obtained, where it is possible to discern low errors on the estimation of both parameters (relative errors below 5%), indicating the feasibility of both methods. In addition, method 1 resulted in lower RMSE for both variables, which can be related to the sensor linearity (since the techniques are based on the linear regression of the sensor's responses) as well as a higher decoupling between variables in method 1, since the pressure variation does not lead to significant variations in the wavelength. Thus, in method 1, the wavelength shift is only related to the pH variation, whereas the amplitude variation is related to both pH and pressure variations.

4. CONCLUSION

This work presented the first optical fiber-embedded smart bandage for wound dressing and healing assessment. A PDMS optical fiber doped with rhodamine B dye was embedded in two wound dressings: a gauze fabric and a hydrocolloid dressing. The pressure sensitivity of the proposed smart bandage is due to high flexibility of the PDMS fiber, which was confirmed by the tensile tests, where Young's modulus of 0.9 MPa was obtained, leading to pressure sensing with high resolution. It is also important to mention that the PDMS fiber stiffness is smaller than the one of gauze fabric (34.0 MPa) and close to the one of hydrocolloid dressing (1.2 MPa). For this reason, the fiber embedded in the wound dressing does not lead to major variations in its stiffness, comfort, and usability. The pH sensing principle is based on the interaction between the rhodamine B dye and the environment pH, where the acidic pH leads to structural changes in the dye due to the spirolactam ring opening in acidic pH. As the rhodamine B dye is included in the fiber structure during its fabrication, the dye-doped PDMS fiber is intrinsically sensitive to pH variations (neutral or acidic). In order to confirm the PDMS and rhodamine B in the fiber molecular structure, FTIR and Raman spectroscopy were conducted, where both analyses indicated the presence of PDMS and rhodamine B in the fiber samples.

The fiber was embedded in the gauze fabric and hydrocolloid dressing, and the transmitted optical power variation was analyzed as a function of the applied pressure, where the results show a high sensitivity and stability of the sensor with capability of measuring pressures as low as 0.1 kPa. Then, the transmitted optical spectrum was analyzed at different pH conditions, indicating a wavelength shift of 0.67 nm/pH when the wavelength peak at 515 nm was analyzed. Furthermore, the smart bandage shows linear variation (R^2 of 0.998) in the transmitted optical power as a function of the environment pH. The sensor analysis also indicates its suitability for dynamic monitoring, where rise and fall times (as a function of the pH variation) of 17.2 s/pH and 31.5 s/pH, respectively, were obtained with a stability of 0.05 pH.

As the sensor is sensitive to both pressure and pH, different techniques for decoupling pH and pressure responses were discussed. One is with two fibers embedded in the bandage in which the transmitted optical power of each fiber is acquired and analyzed. In the other, the transmitted optical spectrum is acquired, where the simultaneous estimation of pH and pressure occurs by the analysis of peak wavelength and optical power in the end facet of the dye-doped PDMS fiber. Therefore, the proposed optical fiber-embedded smart wound dressing has the intrinsic advantages of optical fiber sensors with the possibility of a wearable and low-cost multiparameter monitoring that can be adapted for different wound healing assessment protocols. In one protocol, it is possible to monitor the wound parameters in predefined periods of the day by connecting the fiber to the LS and detector with the additional possibility of using a smartphone as the interrogation unit, since it has a stable source and detector, which were already used in similar applications [34]. The device's flashlight can be used as the white LS and the camera as the PD with the possibility of simultaneous assessment of pH and pressure in both approaches, i.e., with the optical power variations of two embedded fibers (by using space division multiplexing [35]) or with the transmitted optical spectrum (due to novel approaches of smartphone-enabled spectrometers [36]). The proposed smart bandage can also be used in a protocol for continuous monitoring, where the advances in integrated photonics enable the development of on-chip spectrometers and PDs [37], which, in conjunction with a wireless module, can provide the continuous monitoring of pH and pressure. Thus, with the design and results of the proposed optical fiber-embedded smart bandage, it is possible to envisage a next generation of smart wound dressings in which a real-time assessment of the wound healing brings novel paradigms for wound treatments and can dramatically enhance the treatment efficiency. In future works, clinical trials will be conducted, and additional parameters for the smart bandage, such as the assessment of bacterial activity, will be investigated.

Funding. National Natural Science Foundation of China (62003046); Fundação para a Ciência e a Tecnologia (CEECIND/00034/2018, UIDB/50025/2020, UIDP/50025/2020); Petrobras (2017/00702-6); Conselho Nacional de Desenvolvimento Científico e Tecnológico (304049/2019-0, 427054/2018-4); Fundação Estadual de Amparo à Pesquisa do Estado do Espírito Santo (2020-F057G, 84336650).

Acknowledgment. R. Min acknowledges National Natural Science Foundation of China. C. Marques acknowledges Fundação para a Ciência e a Tecnologia (FCT) (iFish project), and this work was developed within the scope of the project i3N, UIDB/50025/2020 & UIDP/50025/2020, financed by national funds through the FCT/MEC. This work is also funded by national funds (OE), through FCT, I.P., in the scope of the framework contract foreseen in the numbers 4, 5, and 6 of the article 23, of the Decree-Law 57/2016, of August 29, changed by Law 57/2017, of July 19.

Disclosures. The authors declare no competing financial and non-financial interests.

REFERENCES

1. C. K. Sen, G. M. Gordillo, S. Roy, R. Kirsner, L. Lambert, T. K. Hunt, F. Gottrup, G. C. Gurtner, and M. T. Longaker, "Human skin wounds: a major and snowballing threat to public health and the economy," Wound Repair Regen. **17**, 763–771 (2009).
2. K. Järbrink, G. Ni, H. Sönnergren, A. Schmidtchen, C. Pang, R. Bajpai, and J. Car, "The humanistic and economic burden of chronic wounds: a protocol for a systematic review," Syst. Rev. **6**, 15 (2017).
3. G. Lagoumintzis, Z. Zagoriti, M. S. Jensen, T. Argyrakos, C. Koutsojannis, and K. Poulas, "Wireless direct microampere current in wound healing: clinical and immunohistological data from two single case reports," Biosensors **9**, 107 (2019).
4. L. Martinengo, N. J. Ying Yeo, Z. Q. Tang, K. D. O. Markandran, B. M. Kyaw, and L. T. Car, "Digital education for the management of chronic wounds in health care professionals: protocol for a systematic review by the digital health education collaboration," J. Med. Internet Res. **8**, e12488 (2019).
5. J. Qu, X. Zhao, Y. Liang, Y. Xu, P. X. Ma, and B. Guo, "Degradable conductive injectable hydrogels as novel antibacterial, anti-oxidant wound dressings for wound healing," Chem. Eng. J. **362**, 548–560 (2019).
6. J. Qu, X. Zhao, Y. Liang, T. Zhang, P. X. Ma, and B. Guo, "Antibacterial adhesive injectable hydrogels with rapid self-healing, extensibility and compressibility as wound dressing for joints skin wound healing," Biomaterials **183**, 185–199 (2018).
7. G. Gethin, "The significance of surface pH in chronic wounds," Wounds UK **3**, 52–56 (2007).
8. L. A. Schneider, A. Korber, S. Grabbe, and J. Dissemond, "Influence of pH on wound-healing: a new perspective for wound-therapy?" Arch. Dermatol. Res. **298**, 413–420 (2007).
9. E. R. Ghomi, S. Khalili, S. N. Khorasani, R. E. Neisiany, and S. Ramakrishna, "Wound dressings: current advances and future directions," J. Appl. Polym. Sci. **136**, 47738 (2019).
10. R. Agha, R. Ogawa, G. Pietramaggiori, and D. P. Orgill, "A review of the role of mechanical forces in cutaneous wound healing," J. Surg. Res. **171**, 700–708 (2011).
11. S. Wang, Q. Zhang, W. Huang, H. Tian, J. Hu, Y. Cheng, and Y. Peng, "A new smart mobile system for chronic wound care management," IEEE Access **6**, 52355–52365 (2018).
12. H. Vu, A. Nair, L. Tran, S. Pal, J. Senkowsky, W. Hu, and L. Tang, "A device to predict short-term healing outcome of chronic wounds," Adv. Wound Care **9**, 312–324 (2020).
13. Y. C. Du and W. S. Ciou, "A sensor gauze with multi-channel moisture and ph monitoring for chronic wound care," IEEE Access **7**, 29185–29192 (2019).
14. C. Broadway, R. Min, A. G. Leal-Junior, C. Marques, and C. Caucheteur, "Toward commercial polymer fiber Bragg grating sensors: review and applications," J. Lightwave Technol. **37**, 2605–2615 (2019).
15. A. G. Leal-Junior, C. A. R. Diaz, L. M. Avellar, M. J. Pontes, C. Marques, and A. Frizera, "Polymer optical fiber sensors in healthcare applications: a comprehensive review," Sensors **19**, 3156 (2019).
16. J. Janting, J. K. M. Pedersen, G. Woyessa, K. Nielsen, and O. Bang, "Small and robust all-polymer fiber Bragg grating based pH sensor," J. Lightwave Technol. **37**, 4480–4486 (2019).
17. A. K. Pathak and V. K. Singh, "A wide range and highly sensitive optical fiber pH sensor using polyacrylamide hydrogel," Opt. Fiber Technol. **39**, 43–48 (2017).
18. X. Cheng, J. Bonefacino, B. O. Guan, and H. Y. Tam, "All-polymer fiber-optic pH sensor," Opt. Express **26**, 14610–14616 (2018).
19. A. L. Aldaba, A. González-Vila, M. Debliquy, M. Lopez-Amo, C. Caucheteur, and D. Lahem, "Polyaniline-coated tilted fiber Bragg gratings for pH sensing," Sens. Actuators B **254**, 1087–1093 (2018).
20. Y. Zhao, M. Lei, S. X. Liu, and Q. Zhao, "Smart hydrogel-based optical fiber SPR sensor for pH measurements," Sens. Actuators B **261**, 226–232 (2018).
21. T. H. Nguyen, T. Venugopalan, T. Sun, and K. T. V. Grattan, "Development of intrinsic optical fiber pH sensors for industrial applications," in *IEEE Sensors* (2009), pp. 89–94.
22. A. Leal-Junior, A. Theodosiou, A. Frizera-Neto, M. J. Pontes, E. Shafir, O. Palchik, N. Tal, S. Zilberman, G. Berkovic, P. Antunes, P. André, K. Kalli, and C. Marques, "Characterization of a new polymer optical fiber with enhanced sensing capabilities using a Bragg grating," Opt. Lett. **43**, 4799–4802 (2018).
23. J. Guo, X. Liu, N. Jiang, A. K. Yetisen, H. Yuk, C. Yang, A. Khademhosseini, X. Zhao, and S. H. Yun, "Highly stretchable, strain sensing hydrogel optical fibers," Adv. Mater. **28**, 10244–10249 (2016).
24. R. Fu, W. Luo, R. Nazempour, D. Tan, H. Ding, K. Zhang, L. Yin, J. Guan, and X. Sheng, "Implantable and biodegradable poly(l-lactic acid) fibers for optical neural interfaces," Adv. Opt. Mater. **6**, 1700941 (2018).
25. J. Guo, M. Niu, and C. Yang, "Highly flexible and stretchable optical strain sensing for human motion detection," Optica **4**, 1285–1288 (2017).
26. J. Guo, K. Zhao, B. Zhou, W. Ning, K. Jiang, C. Yang, L. Kong, and Q. Dai, "Wearable and skin-mountable fiber-optic strain sensors interrogated by a free-running, dual-comb fiber laser," Adv. Opt. Mater. **7**, 1900086 (2019).
27. H. S. Lv, S. Y. Huang, B. X. Zhao, and J. Y. Miao, "A new rhodamine B-based lysosomal pH fluorescent indicator," Anal. Chim. Acta **788**, 177–182 (2013).
28. H. N. Kim, M. H. Lee, H. J. Kim, J. S. Kim, and J. Yoon, "A new trend in rhodamine-based chemosensors: application of spirolactam ring-opening to sensing ions," Chem. Soc. Rev. **37**, 1465–1472 (2008).
29. A. G. Leal-Junior, A. Frizera, and M. J. Pontes, "Analytical model for a polymer optical fiber under dynamic bending," Opt. Laser Technol. **93**, 92–98 (2017).
30. E. Smith and G. Dent, *Modern Raman Spectroscopy—A Practical Approach* (Wiley, 2005).
31. H. I. C. Harn, R. Ogawa, C. K. Hsu, M. W. Hughes, M. J. Tang, and C. M. Chuong, "The tension biology of wound healing," Exp. Dermatol. **28**, 464–471 (2019).
32. A. Leal-Junior, A. Frizera, C. Díaz, C. Marques, M. Ribeiro, and M. J. Pontes, "Material features based compensation technique for the temperature effects in a polymer diaphragm-based FBG pressure sensor," Opt. Express **26**, 20590–20602 (2018).
33. A. G. Leal-Junior, A. Theodosiou, C. Diaz, C. Marques, M. J. Pontes, K. Kalli, and A. Frizera, "Simultaneous measurement of axial strain, bending and torsion with a single fiber Bragg grating in CYTOP fiber," J. Lightwave Technol. **37**, 971–980 (2018).
34. A. Sultangazin, J. Kusmangaliyev, A. Aitkulov, D. Akilbekova, M. Olivero, and D. Tosi, "Design of a smartphone plastic optical fiber chemical sensor for hydrogen sulfide detection," IEEE Sens. J. **17**, 6935–6940 (2017).
35. A. G. Leal-Junior, A. Frizera, C. Marques, and M. J. Pontes, "Optical fiber specklegram sensors for mechanical measurements: a review," IEEE Sens. J. **20**, 569–576 (2020).
36. M. A. Hossain, J. Canning, K. Cook, and A. Jamalipour, "Optical fiber smartphone spectrometer," Opt. Lett. **41**, 2237–2240 (2016).
37. Z. Wang, S. Yi, A. Chen, M. Zhou, T. S. Luk, A. James, J. Nogan, W. Ross, G. Joe, A. Shahsafi, K. X. Wang, M. A. Kats, and Z. Yu, "Single-shot on-chip spectral sensors based on photonic crystal slabs," Nat. Commun. **10**, 1020 (2019).